Received: 18 April 2022 | Revised: 3 August 2022 | Accepted: 20 August 2022 | Published online: 2 October 2022

DOI: 10.1002/trc2.12356

Alzheimer's & Dementia
Translational Research & Clinical Interventions

RESEARCH ARTICLE

Free water derived by multi-shell diffusion MRI reflects tau/neuroinflammatory pathology in Alzheimer's disease

Moto Nakaya[1,2] | Noriko Sato[1] | Hiroshi Matsuda[1,3] | Norihide Maikusa[1] | Yoko Shigemoto[1] | Daichi Sone[4,5] | Tensho Yamao[6] | Masayo Ogawa[5] | Yukio Kimura[1] | Emiko Chiba[1] | Masahiro Ohnishi[1] | Koichi Kato[5] | Kyoji Okita[5] | Tadashi Tsukamoto[7] | Yuma Yokoi[8] | Masuhiro Sakata[8] | Osamu Abe[2]

[1]Department, of Radiology, National Center Hospital of Neurology and Psychiatry, Ogawa-Higashi, Kodaira, Tokyo, Japan

[2]Department of Radiology, Graduate School of Medicine, University of Tokyo, Hongo, Bunkyo-ku, Tokyo, Japan

[3]Drug Discovery and Cyclotron Research Center, Southern TOHOKU Research Institute for Neuroscience, Koriyama, Japan

[4]Department of Psychiatry, The Jikei University School of Medicine, Tokyo, Japan

[5]Integrative Brain Imaging Center, National Center of Neurology and Psychiatry, Tokyo, Japan

[6]Department of Radiological Sciences, School of Health Sciences, Fukushima Medical University, Fukushima, Japan

[7]Department of Neurology, National Center of Neurology and Psychiatry, Kodaira, Tokyo, Japan

[8]Department of Psychiatry, National Center of Neurology and Psychiatry, Kodaira, Tokyo, Japan

Correspondence
Noriko Sato, Department of Radiology, National Center Hospital of Neurology and Psychiatry, 4-1-1, Ogawa-Higashi, Kodaira, Tokyo, 187-8551, Japan.
Email: snoriko@ncnp.go.jp

Abstract

Introduction: Free-water (FW) imaging, a new analysis method for diffusion magnetic resonance imaging (MRI), can indicate neuroinflammation and degeneration. We evaluated FW in Alzheimer's disease (AD) using tau/inflammatory and amyloid positron emission tomography (PET).

Methods: Seventy-one participants underwent multi-shell diffusion MRI, ^{18}F-THK5351 PET, ^{11}C-Pittsburgh compound B PET, and neuropsychological assessments. They were categorized into two groups: healthy controls (HCs) (n = 40) and AD-spectrum group (AD-S) (n = 31) using the Centiloid scale with amyloid PET and cognitive function. We analyzed group comparisons in FW and PET, correlations between FW and PET, and correlation analysis with neuropsychological scores.

Results: In AD-S group, there was a significant positive correlation between FW and ^{18}F-THK5351 in the temporal lobes. In addition, there were negative correlations between FW and cognitive function in the temporal lobe and cingulate gyrus, and negative correlations between ^{18}F-THK5351 and cognitive function in the same regions.

Discussion: FW imaging could be a biomarker for tau in AD alongside clinical correlations.

KEYWORDS
Alzheimer's disease, free-water imaging, Centiloid scale, amyloid, tau

1 | BACKGROUND

Alzheimer's disease (AD) is the most common neurodegenerative disorder, characterized by senile plaques and neurofibrillary changes composed of amyloid beta (Aβ) and tau proteins.[1] Recent studies have demonstrated that Aβ interacts with cortical tau pathology to influence neurodegeneration,[2–4] Because neurodegenerative processes involving Aβ and tau appear years before clinical symptoms, their evaluation has become an important issue in AD research.[5] Although the clinical diagnosis of AD is based on the clinical course and symptoms of

neuropsychological tests, diagnostic imaging of the brain has become an essential complement to research criteria. New diagnostic criteria based on the presence or absence of amyloid, tau, and neuronal injury have been proposed by using positron emission tomography (PET) and biomarkers.[6]

In vivo molecular neuroimaging with PET is a powerful and minimally invasive tool for measuring specific molecules and metabolism in the brain. Amyloid PET scans are used to test and monitor clinical therapies for modifying AD and to aid in clinical diagnosis and prognosis.[7] Attempts have been made to quantitatively standardize the results of amyloid PET examinations due to variations in tracers, PET scanners, procedural factors, and analysis methods at various imaging centers. Klunk et al.[8] used Centiloid units (CLs) to standardize the reporting of amyloid imaging. They derived a scale called the CL that has values ranging from 0 to 100, where 0 represents young healthy controls (HCs), and 100 represents the amyloid burden found in mild to moderate cases of dementia due to AD, across anchor points. This provides comparable data for amyloid PET studies at different sites and across different amyloid tracers. Combining CL with standardized amyloid PET accumulation and neuropsychological assessments allows us to objectively recognize HCs, pre-clinical AD, mild cognitive impairment (MCI), and AD. The recent development of tau PET has provided new and useful information about AD and other tauopathies.[9,10] Tau deposition has been shown to be associated with focal gray matter loss in both AD and amyloid-negative older adults.[11,12] One of the first generation of tau tracers, ^{18}F-THK5351, is distributed in tau-related regions of AD[13]; however, due to off-target binding to monoamine oxidase,[14] ^{18}F-THK5351 does not purely reflect tau pathology. ^{18}F-THK5351 is now considered to target tau aggregation as well as neuroinflammation associated with astrogliosis.[15]

Magnetic resonance imaging (MRI) has been used as a clinical tool to identify early cognitive decline and stages in AD.[16] Free-water (FW) imaging is a recently developed measurement for diffusion MRI; it measures the fraction of diffusion signals explained by isotopically unrestricted water, as estimated from a regularized bi-tensor model.[17] Elevated FW in the extracellular space around axons may suggest neuroinflammation and association with AD.[18] Furthermore, FW in the corpus callosum, cingulate gyrus, and frontal, temporal, and parietal lobes is significantly correlated with cerebrospinal fluid (CSF) biomarkers such as Aβ42, phosphorylated tau 181 (p-tau181), neurofilament light chain protein, YKL-40, and monocyte chemoattractant protein 1.[19–21] FW has also been reported in many other neurological disorders, such as Parkinson's disease[22] and schizophrenia.[23]

We previously showed that tau and neuroinflammation in AD might decrease neurite density and orientation dispersion, specifically in the medial and lateral temporal lobes.[24] However, there have been no reports examining the correlation between FW and ^{18}F-THK5351 in AD. We hypothesized that FW would also increase in areas where ^{18}F-THK5351 was deposited. In this study, we examined the relationship between FW imaging, ^{18}F-THK5351 PET, and ^{11}C-Pittsburgh compound B (PiB) PET in patients with AD spectrum group (AD-S) and HCs classified based on neuropsychological measurements and CL using amyloid PET.

RESEARCH IN CONTEXT

1. **Systematic review**: The authors reviewed the literature using sources such as PubMed. Free-water (FW) imaging of Alzheimer's disease (AD) has not been studied as extensively as other magnetic resonance imaging (MRI) tools such as diffusion tensor imaging. However, several recent publications describe FW imaging. These relevant studies have been cited appropriately.
2. **Interpretation**: FW imaging reflects the pathophysiology of AD and may represent a potential related biomarker to ^{18}F-THK5351. This may allow us to use MRI, which is convenient and economical, instead of positron emission tomography (PET) for staging evaluation of AD.
3. **Future directions**: In this article we propose a framework for generating new hypotheses and conducting additional research. For example, (1) correlation between FW imaging and second-generation tau tracers, (2) correlation between FW imaging and neuroinflammation-specific imaging associated with astrogliosis, and (3) the superiority of FW imaging compared to past MRI tools.

2 | MATERIAL AND METHODS

2.1 | Participants

Ninety-three participants were recruited for this prospective study from the National Center of Neurology and Psychiatry between 2014 and 2018. For inclusion criteria, participants 55 years of age or older were recruited with the exclusion of those with comorbid chronic diseases, a history of central nervous system disease, including vascular diseases, severe head trauma, or those meeting the criteria for substance abuse/dependence. The participants included amyloid negative, normal cognitive HCs, and amyloid-positive patients as AD-S. A 3.0 T MRI (including three-dimensional [3D] T1-weighted imaging and multi-shell diffusion imaging), ^{11}C-PiB and ^{18}F-THK5351 PET, and neuropsychological tests were performed on the subjects. Furthermore, we excluded patients with cognitive decline and no evidence of amyloid to determine the HC group from those considered clinically healthy, which made the distinct grouping of AD possible. The remaining 71 participants were classified into two groups. The groups were determined using neuropsychological tests and amyloid PET by the CL of the target cortex determined according to the protocol in the Global Alzheimer's Association Interactive Network (http://www.gaain.org/centiloid-project) as follows: HC group with participants who were amyloid negative and had a Clinical Dementia Rating (CDR) of 0 ($N = 40$), and AD-S group with participants who were amyloid positive ($N = 31$).

This cross-sectional observational study was approved by the institutional review board of the National Center of Neurology and

Psychiatry. All participants provided written informed consent prior to participation.

2.2 | Clinical and neuropsychological assessments

The age, sex, and education of the participants were noted. They underwent Clinical Dementia Rating Sum of Boxes (CDR-SB), Mini-Mental State Examination (MMSE), Japanese version of Montreal Cognitive Assessment (MoCA-J), and Frontal Assessment Battery (FAB). FAB scores could not be collected in 2 cases in the AD-S group, and 15 cases in the HC group.

2.3 | Image acquisition

Participants underwent MRI scanning on a 3.0 T MRI system (Verio, Siemens, Erlangen, Germany). Three-dimensional sagittal T1-weighted magnetization prepared rapid acquisition with gradient echo (MPRAGE) images were obtained with the following scanning parameters: repetition time (TR)/echo time (TE) of 1900 ms/2.52 ms, 9° flip angle (FA), 1.0 × 1.0 mm in-plane resolution, 1.0 mm effective slice thickness with no gap, 300 slices, 256 × 256 matrix, and 25 × 25 cm field of view (FOV). For FW imaging, the images using multi-shell diffusion were acquired along 30 non-collinear directions at three *b*-values (0, 1000, and 2000 s/mm^2). Furthermore, two images with reversed-phase encoding (blip up/down) were acquired without any diffusion gradient. The diffusion MRI parameters were as follows: TR/TE of 17700 ms/93 ms, 90°FA, 2.0 × 2.0 mm in-plane resolution, 2.0 mm effective slice thickness, 74 slices, 114 × 114 matrix, and 22.4 × 22.4 cm FOV.

PET/computed tomography (CT) scans were performed on a Siemens/Biograph 16 scanner (3D acquisition mode, 81 image planes, 16.2 cm axial FOV. 4.2 mm transaxial resolution, 4.7 mm axial resolution, and 2-mm slice interval). A low-dose CT scan was performed for attenuation correction. ^{11}C-PiB at a dose of 555 MBq was injected intravenously 50 minutes before the PET/CT scan for ^{11}C-PiB imaging. The emission scan duration was 20 minutes. ^{18}F-THK5351 was injected 40 minutes before the ^{18}F-THK5351 scan at a dose of 185 MBq. The scan duration was 20 minutes. PET/CT images were reconstructed using a combination of Fourier rebinning and Ordered Subsets Expectation. The interval average and SD between ^{18}F-THK5351, ^{11}C-PiB PET, and MRI was 22.1 ± 23.0 days (^{18}F-THK5351 to ^{11}C-PiB: 12.2 ± 15.7 days, ^{18}F-THK5351 to MRI: 13.8 ± 17.5 days, and ^{11}C-PiB to MRI: 18.3 ± 23.8 days).

2.4 | FW imaging and FW-corrected DTI maps processing

The FW imaging and FW-corrected fractional anisotropy $(FA)_T$ images were generated from eddy current corrected volumes by fitting the FW model[17,25,26] using the "Using the free water elimination model to remove Diffusion Tensor Imaging (DTI) free water contamination" script (https://dipy.org/documentation/1.0.0./examples_built/reconst_fwdti/) that was executed using Diffusion Imaging in Python ver 1.0 (DIPY, https://dipy.org). It includes a de-noising approach based on the Marchenko-Pastur Principal Component Analysis method.[27] The images were also co-registered to the T1-weighted images and normalized to the Montreal Neurological Institute (MNI) space using the Diffeomorphic Anatomical Registration Through Exponentiated Lie (DARTEL) method.[28] We removed as much of the influence as possible by shaving the CSF and skull, thereby creating a mask in the analysis. Smoothing was performed with an 8 mm full-width at half-maximum (FWHM) Gaussian kernel. We used Statistical Parametric Mapping 12 software (SPM12; http://www.fil.ion.ucl.ac.uk/spm /) for the series of processes referred to in previous literature.[24] We visually checked the masking out in each test to avoid potential noise from the CSF.

2.5 | PET processing

After partial volume correction using the PETPVE12 toolbox,[29] the ^{11}C-PiB and ^{18}F-THK5351 PET images were spatially normalized using SPM. The PET images of the participants were co-registered to their T1-weighted images and spatially normalized to the MNI space using the DARTEL method.[28] After spatial normalization, all PET images were divided by the positive mean uptake value of the cerebellar gray matter of an individual. Standardized uptake value ratio (SUVR) images were obtained, and each image was smoothed using an 8-mm FWHM Gaussian kernel. SUVR is calculated from standardized subject PET counts in the cerebral cortex (GAAIN Pons VOI).[30] Finally, SUVR was converted to CL values using the direct conversion equation for each PET tracer. We used a cut-off value of 10 for CL[31] to classify positive and negative amyloid accumulation. In this study, we used a stand-alone software for quantifying amyloid PET to calculate CL.[30]

2.6 | Voxel-wise directed correlations between FW imaging and PET imaging

We used the VoxelStats toolbox[32] to estimate the relationship between FW imaging and PET. Using a general linear model, the toolbox calculated voxel-wise correlations between the two imaging modalities with age, sex, and years of education as covariates. We analyzed the correlations between FW and PET-related imaging modalities, including FW imaging and ^{18}F-THK5351/^{11}C-PiB. These analyses were performed separately for the AD-S and HC groups. BrainNet Viewer (http://www.nitrc.org/projects/bnv/) was used to visualize the results.[33]

2.7 | Statistics

To compare the clinical demographics between the AD-S and HC groups, we used an unpaired *t*-test for continuous variables and Pearson chi-square test for categorical parameters in JMP Pro ver.

TABLE 1 Demographics of the AD-S and HC groups in this study

	AD-S group ($N = 31$)	HC group ($N = 40$)	P
Age [years, mean ± SD (range)]	70.4 ± 8.0	65.5 ± 8.7	.07[b]
Sex (F:M)	20:11	20:20	.22[c]
Education, y (mean ± SD)	13.5 ± 2.6	14.4 ± 2.4	.11[b]
CDR-SOB (mean ± SD)	3.3 ± 3.1	all 0	–
MMSE (mean ± SD)	23.6 ± 4.7	29.3 ± 1.1	<.001[b]
MoCA (mean ± SD)	20.4 ± 6.2	27.1 ± 2.2	<.001[b]
FAB (mean ± SD)	14.0 ± 2.6[a]	16.5 ± 2.1[a]	<.001[b]
SUVR of 11C-PiB within whole cortex (mean ± SD)	1.81 ± 0.51	0.97 ± 0.04	<.001[b]
CL of 11C-PiB whole cerebellum (mean ± SD)	75.5 ± 48.4	−3.2 ± 3.9	–

Abbreviations: AD-S, Alzheimer's disease spectrum; CDR, Clinical Dementia Rating; CL, Centiloid; FAB, Frontal Assessment Battery; HCs; healthy controls; MMSE, Mini-Mental State Examination; MoCA-J, Japanese version of Montreal Cognitive Assessment; *N*, number of participants; SUVR, standardized uptake value ratio.

[a]Two cases in the AD-S group and 15 cases in the HC group could not be collected.

[b]*t*-test.

[c]χ^2 test.

15.0.0 (SAS Institute Inc., Cary, NC, USA). Statistical significance was set at $P < .05$.

For whole-brain SPM12 analyses (i.e., group comparison in FW, FA_T, and PET, and correlation analysis with neuropsychological scores), we used a two-sample *t*-test and multiple regression designs, using age, sex, and years of education as covariates. Results with a height threshold of $P < .001$ (uncorrected) and clusters were considered as significant when falling below a cluster corrected *P* (family wise error [FWE]) = .05 were considered significant.

For correlations between different imaging modalities, VoxelStats generated results based on random field theory (RFT) correction.[32] The significance level was set at $P < .001$ (RFT-corrected).

3 | RESULTS

3.1 | Demographics in AD-S and HC groups

Table 1 summarizes the demographics, neuropsychological assessments, SUVR, and CL in each group. There were no statistically significant differences in age, sex, or years of education among the two groups.

3.2 | Group differences in FWI, FW-corrected DTI maps, and ^{11}C-PiB and ^{18}F-THK5351 PET studies

FW increased predominantly in the hippocampus, parahippocampal, and fusiform gyrus in the AD-S group as compared to the HC group

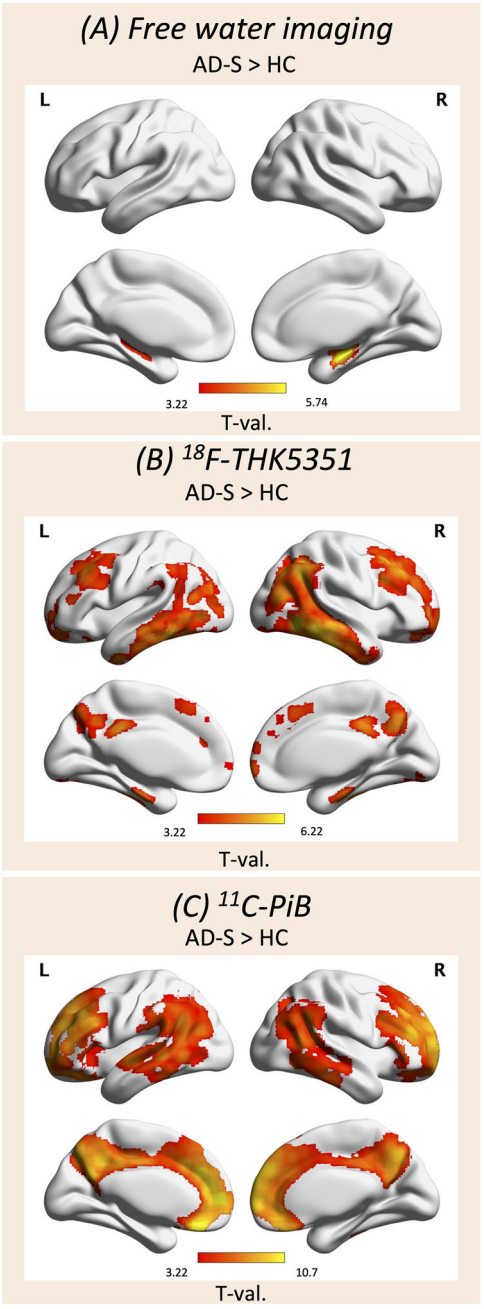

FIGURE 1 Group differences in the free water (FW) imaging and positron emission tomography (PET) study; *t*-test among the three groups (A, B, and C). Group differences between the Alzheimer's disease spectrum (AD-S) and healthy control (HC) groups in FW imaging (A), ^{18}F-THK5351 (B), and ^{11}C-PiB (C) studies. Color bars denote statistically significant T-values from minimum to maximum.

(Figure 1A). In the ^{18}F-THK5351 PET study, there was a significant increase in the frontal lobe, temporal lobe, and posterior cingulate gyrus in the AD-S group, as compared to the HC group (Figure 1B). In the ^{11}C-PiB PET study, there was a significant increase in the frontal lobes, lateral temporal lobes, and posterior cingulate gyrus in the AD-S group, as compared to the HC group (Figure 1C). In FA_T, the clusters of $P < .05$ (FWE corrected) were not significantly different, unlike FW.

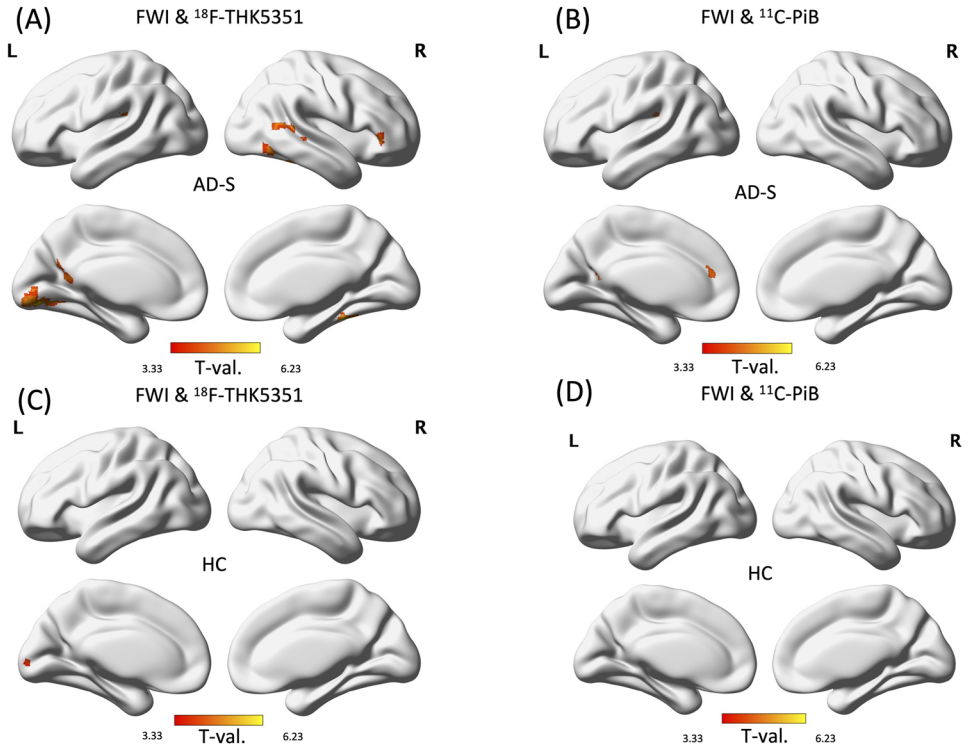

FIGURE 2 Voxel-wise correlations between free water (FW) imaging and positron emission tomography (PET). (A) Positive correlations between FW imaging and ^{18}F-THK5351 in the Alzheimer's disease spectrum (AD-S) group, (B) positive correlations between FW imaging and ^{11}C-PiB in the AD-S group, no correlations (C) between FW imaging and ^{18}F-THK5351, and (D) FW imaging and ^{11}C-PiB in the health control (HC) group. Color bars denote the statistically significant T-values from minimum to maximum.

The results for a voxel-level height threshold of $P < .001$ (uncorrected) are attached in the Supplement 1B.

3.3 | Image correlations between FW imaging and PET

In the AD-S group, there was a significant positive correlation between FW and ^{18}F-THK5351 in the temporal and posterior cingulate gyri (Figure 2A). There were no significant correlations between ^{11}C-PiB and FW in the AD-S group (Figure 2B). In the HC group, there were no significant correlations between FW and ^{18}F-THK5351 or FW and ^{11}C-PiB (Figure 2C,D).

3.4 | Correlations with neuropsychological measurements in FW and PET studies

For MoCA-J, FW imaging showed significant negative correlations in the temporal lobes and prefrontal cortex for the AD-S group only (Figure 3A). ^{18}F-THK5351 imaging also showed significant negative correlations in the temporal lobes and prefrontal cortex (Figure 3B), whereas ^{11}C-PiB showed no significant correlations (Supplement 2A). For FAB, both FW imaging and ^{18}F-THK5351 detected negative correlations in the bilateral lateral parietal lobes, posterior cingulate gyri, and precuneus (Figure 3C,D). ^{11}C-PiB did not show significant correlations for any group (Supplement 2B). For MMSE, FW imaging showed a negative correlation in the temporal lobe in the AD-S group; however, neither ^{18}F-THK5351 nor ^{11}C-PiB showed a correlation even in the AD-S group (Supplement 3). FW imaging, ^{18}F-THK5351, and 1PiB showed no correlation with MMSE in the HC group.

4 | DISCUSSION

To the best of our knowledge, this is the first study to examine the voxel-wise image correlation between FW imaging and ^{18}F-THK5351 or ^{11}C-PiB in subgroups classified by CL. There was a positive correlation between FW imaging and ^{18}F-THK5351 in the AD-S group, mainly in the temporal lobe, suggesting that tau aggregation and neuroinflammatory processes in these regions might elevate the extracellular FW of brain tissue in AD. In the correlations between neurological examinations and FW imaging or ^{18}F-THK5351, there were correlation between similar distributions in regions such as the temporal lobe, posterior cingulate gyrus, and precuneus. We believe these relationships indicate that FW imaging adequately reflects the pathology of AD and can be a related biomarker to ^{18}F-THK5351.

Previous reports have shown little association between gray matter atrophy on MRI and ^{18}F-THK5351 accumulation in patients with AD, even with partial volume correction.[34] This discrepancy indicates

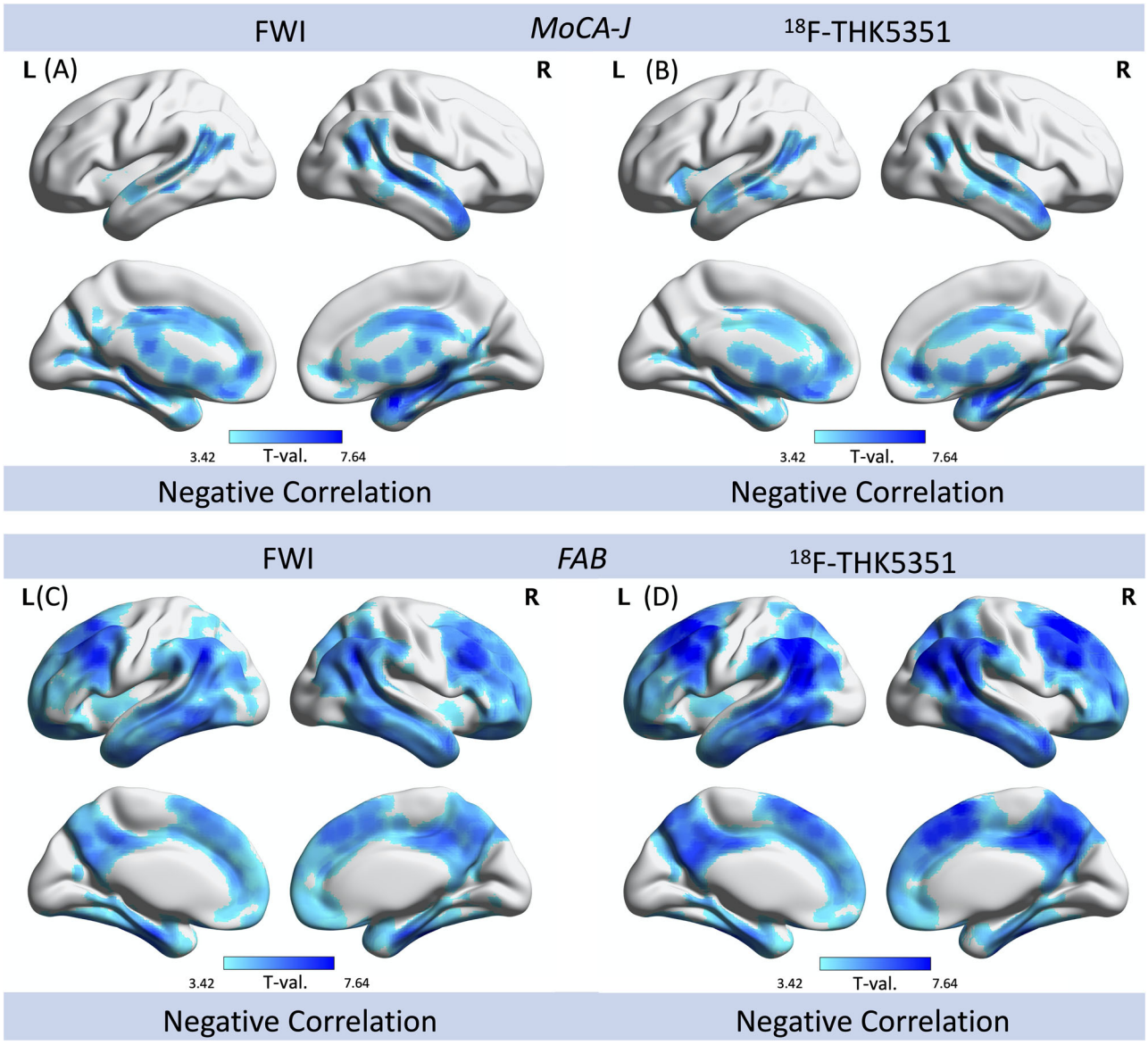

FIGURE 3 Free water (FW) and ^{18}F-THK5351 imaging correlations with the Japanese version of Montreal Cognitive Assessment (MoCA-J) and frontal assessment battery (FAB) in Alzheimer's disease spectrum (AD-S) correlations with MoCA-J in (A) FW imaging and (B) ^{18}F-THK5351, with FAB in (C) FW imaging and (D) ^{18}F-THK5351 in the AD-S group. Color bars denote statistically significant T-values from minimum to maximum.

that ^{18}F-THK5351 accumulation precedes atrophy, suggesting that tau PET may provide important information at an earlier stage than morphologic study by MRI.[9] According to the pathological theory of AD,[1] neurofibrillary tangles first target the temporal lobe outside the hippocampus and damage the hippocampus through the perforant pathway. Therefore, the lateral and medial temporal lobes, where we found significant association between FW and ^{18}F-THK5351, would be the regions that are most susceptible to the effects of tau accumulation (Figure 2A). An important role of tau is to mediate Aβ toxicity at the post-synapse level.[35] Recent studies have demonstrated that Aβ interacts with cortical tau pathology to influence neurodegeneration.[2] Aβ toxicity is expected to cause inflammatory changes with FW. Therefore, the association between ^{18}F-THK5351 and FW in the present study may have a significant impact on neurodegeneration in AD. Although the distribution of ^{18}F-THK5351 reflects the severity of AD, Aβ accumulates mainly in the neocortex and has been found to be less associated with AD progression and cognitive impairment.[1,36] In addition, ^{18}F-THK5351 PET was reported to be useful for monitoring neuroinflammatory processes in the brain.[37] We found that FW imaging correlated more broadly with ^{18}F-THK5351 than with ^{11}C-PiB in the posterior cingulate gyrus and temporal lobe, suggesting that FW can be a biomarker for the progression of AD-related inflammation and degeneration. Abnormalities in FW can be associated with neuroinflammatory processes, because previous reports have shown that FW imaging is useful as a marker of progression in pre-clinical and symptomatic AD, is significantly correlated with CSF

biomarkers such as YKL-40 in AD, and is associated with changes in neuroinflammation.[20,38]

In the present study the groups were divided by CL, which was determined according to the protocol described by Klunk et al.[8] This study is the first report on FW imaging using the Centiloid scale to classify AD groups. Proper interpretation of PiB-PET findings requires a clear understanding of relationships between PET data and background Aβ neuropathology. In a previous FW imaging study for AD, one report assessed patients by SUVR rather than CL, which might not be an accurate scaling for amyloid deposition, although amyloid PET was also used.[19] Others defined AD patients based on clinical evaluations, without examination of amyloid deposition.[39,40] Several autopsy studies have found that significant Aβ deposition is present in more than 30% of cognitively normal older adults post-mortem, indicating that the extent of Aβ pathology may not be distinct from that found in AD.[41] According to a report, the assessment of the level of Aβ deposition as defined by CL was important in predicting progression to MCI and dementia.[42] In the present study, we used a cut-off value of 10 for CL[31] to classify positive and negative amyloid accumulation. Furthermore, we excluded patients with cognitive decline to determine the HC group from those considered clinically healthy, which would make the distinct grouping of AD possible. We observed clear significant differences in the frontal lobe, posterior cingulate gyrus, precuneus, parietal lobe, and lateral temporal lobe in the group comparison between AD-S and HC group for ^{11}C-PiB.

We further investigated the association with neuropsychological measures. Ji et al.[39] showed an association between FW and impaired attention, cognitive performance, executive function, and visual construction in patients with AD and MCI, supporting the idea that FW is associated with clinical symptoms. They assessed the correlations between the mean FW of white matter regions of the whole brain and CDR. In this study, we assessed the cortical distribution in whole-brain analysis. We observed that FW correlated with cognitive function, particularly in the temporal lobe in the AD-S group (Figure 3). For ^{18}F-THK5351, a correlation was also found with all scores of all MoCA-J, FAB, and MMSE tests in the AD-S group, which was consistent with previous literature on tau PET.[36] Elevated FW was associated with cognitive function in the temporal lobe, frontal lobe, and posterior cingulate gyrus (Figure 3). Moreover, the correlations between ^{18}F-THK5351 and FW and these neuropsychological tests were similar in the regions of the whole-brain analysis, and no significant correlation was observed in ^{11}C-PiB. Tau and inflammatory pathology in these regions might affect the cognitive functions in AD, which is correlated with FW content. This suggests that neurofibrillary change pathology in AD is highly correlated with cognitive dysfunction,[43,44] whereas senile plaque pathology is not correlated with the clinical severity stage.[45]

Many studies on diffusion MRI in AD have focused primarily on changes in the white matter.[46] Some reports have presented the relationship between Aβ deposition and white matter pathology by DTI.[47,48] In addition, evaluation of white matter changes by DTI has been reported to be useful in the evaluation of the stage of AD.[49,50] However, cerebral gray matter is impaired very early in AD, and pathology suggests that gray matter changes precede white matter changes.[51] FW imaging is useful in the assessment of gray and white matter. Contrary to patients with AD, FWI detected the white matter microstructure changes preceding in the gray matter of patients with PD.[52] There is direct evidence of altered FW, which may be related to neurodegeneration-related atrophy, cell loss, and neuroinflammation in PD.[53,54] Neuroinflammation and glial activation are being recognized increasingly as early events in AD, even before Aβ deposition.[55] The increase in cortical FW is expected during the symptomatic phase of AD and may be due to the disruption of microstructural barriers such as myelin cell membranes and intracellular organelles, which normally restrict the movement of water molecules and the blood-brain barrier associated with neuroinflammation.[38,51] In contrast, ^{18}F-THK5351 generally has a high uptake into the gray matter. In fact, unlike ^{11}C-PiB, the group differences in FW imaging and neuropsychological correlations in this study were like those of ^{18}F-THK5351, which targeted not only tau aggregation but also neuroinflammation associated with astrogliosis.[15] Considering that ^{18}F-THK5351 is generally taken up by gray matter,[56] it might become a biomarker comparable to tau-related PET in the diagnosis and disease monitoring of AD.

Previous reports have obtained FW imaging using single-shell diffusion MRI data,[19,20] whereas in this study, it was obtained using multi-shell diffusion MRI data, which is more robust.[57] Another advantage of this study is that diffusion images were collected on a single machine at a single site. Diffusion MRI data, originally obtained at different sites and machines, are subject to high inter- and intra-scanner variability for several reasons, including head coil sensitivity, nonlinearity of imaging gradients, magnetic field inhomogeneity, and other scanner-related factors. Although many studies were multi-center and used multiple machines,[19–21] this study had advantages such as absence of variability among multi-center and multi-machine diffusion MRI data.

This study has several limitations. First, although ^{18}F-THK5351 is thought to reflect the combined pathology of tau and inflammation associated with astrogliosis,[16] we were unable to assess these two mechanisms separately. Future studies using second-generation tau tracers and neuroinflammation-specific imaging should provide more relevant insights. Second, the effect of CSF in the sulcus associated with brain atrophy could not be completely ruled out. In earlier studies, techniques using gray matter–based spatial statistics have been reported.[58] However, as an alternative, we removed the influence as much as possible by shaving the CSF and skull, thereby creating a mask in the analysis. In addition, because the whole-brain analysis and assessment were performed in cluster levels, the influence of errors on the brain surface is minimal. Third, the influence of partial volume effects cannot be ruled out. This is a major limitation of any study using diffusion sequence with standard resolution for detecting differences in the cortex. Fourth, it was reported that microstructure alterations and p-tau181/Aβ42 were associated,[59] although we did not search for such CSF biomarkers.

We found a positive correlation between ^{18}F-THK5351 and FW in AD-S brains. This suggests that tau and neuroinflammatory pathologies elevate FW, specifically in the medial and lateral temporal lobes.

Combined with the clinical correlation results, these indicate that FW can be a related biomarker to tau and/or neuroinflammatory pathologies.

ACKNOWLEDGMENTS

The authors would like to thank Dr. Etsuko Imabayashi for her practical support and academic advice. Furthermore, we also thank Editage (www.editage.jp) for English-language editing. This work was partly carried out under the Brain Mapping by Integrated Neurotechnologies for Disease Studies (Brain/MINDS) project (grant number 16dm0207017h0003), funded by the Japan Agency for Medical Research and Development (AMED), and an Intramural Research (Grant No. 3-3 and 3-10) for Neurological and Psychiatric Disorders from the National Center of Neurology and Psychiatry.

CONFLICT OF INTEREST

None declared. Author disclosures are available in the supporting information.

REFERENCES

1. Braak H, Braak E, Neuropathological staging of Alzheimer-related changes. *Acta Neuropathol* 1991;82:239-259.
2. Wang L, Benzinger TL, Su Y, et al. Evaluation of tau imaging in staging Alzheimer disease and revealing interactions between β-amyloid and tauopathy. *JAMA Neurol*. 2016;73(9):1070-7.
3. Fortea J, Vilaplana E, Alcolea D, et al. Alzheimer's disease neuroimaging initiative, cerebrospinal fluid β-amyloid and phospho-tau biomarker interactions affecting brain structure in preclinical Alzheimer disease. *Ann Neurol*. 2014;76(2):223-30.
4. Pascoal TA, Mathotaarachchi S, Mohades S, et al. Amyloid-β and hyperphosphorylated tau synergy drives metabolic decline in preclinical Alzheimer's disease. *Mol Psychiatry*. 2017;22(2):306-311.
5. Jack CR Jr, Knopman DS, Jagust WJ, et al. Hypothetical model of dynamic biomarkers of the Alzheimer's pathological cascade. *Lancet Neurol*. 2010;9:119-128.
6. Jack CR, Bennett DA, Blennow K, et al. NIA-AA research framework: toward a biological definition of Alzheimer's disease. *Alzheimers Dement* 2018;14:535-562.
7. Johnson KA, Minoshima S, Bohnen NI, et al. Appropriate use criteria for amyloid PET: a report of the amyloid imaging task force, the society of nuclear medicine and molecular imaging, and the Alzheimer's association. *Alzheimers Dement* 2013;9:e1-e16.
8. Klunk WE, Koeppe RA, Price JC, et al. The Centiloid Project: standardizing quantitative amyloid plaque estimation by PET. *Alzheimers Dement* 2015;11(1):1-15.e4.
9. Matsuda H, Shigemoto Y, Sato N, Neuroimaging of Alzheimer's disease: focus on amyloid and tau PET. *Jpn J Radiol* 2019;37:735-749.
10. Leuzy A, Chiotis K, Lemoine L, et al. Tau PET imaging in neurodegenerative tauopathies-still a challenge. *Mol Psychiatry* 2019;24:1112-1134.
11. Shigemoto Y, Sone D, Ota M, et al. Voxel-based correlation of 18 F-THK5351 accumulation and gray matter volume in the brain of cognitively normal older adults. *EJNMMI Research*. 2019;9:81.
12. Acosta-Cabronero J, Nestor PJ. Diffusion tensor imaging in Alzheimer's disease: insights into the limbic-diencephalic network and methodological considerations. *Front Aging Neurosci* 2014;6:266.
13. Betthauser TJ, Lao PJ, Murali D, et al. In vivo comparison of tau radioligands 18F-THK-5351 and 18F-THK-5317. *J Nucl Med* 2017;58:996-1002.
14. Ng KP, Pascoal TA, Mathotaarachchi S, et al. Monoamine oxidase B inhibitor, selegiline, reduces 18F-THK5351 uptake in the human brain. *Alzheimers Res Ther* 2017;9:25.
15. Okamura N, Harada R, Ishiki A, et al. The development and validation of tau PET tracers: current status and future directions. *Clin Transl Imaging* 2018;6:305-316.
16. Doherty BM, Schultz SA, Oh JM, et al. Amyloid burden, cortical thickness, and cognitive function in the Wisconsin Registry for Alzheimer's Prevention. *Alzheimers Dement (Amst)* 2015;1:160-169.
17. Pasternak O, Sochen N, Gur Y, et al. Free water elimination and mapping from diffusion MRI. *Magn Reson Med* 2009;62:717-730.
18. Pasternak O, Shenton M, Westin CF et al. Estimation of extracellular volume from regularized multi-shell diffusion MRI. *Med Image Comput Assist Interv* 2012;15:305-312.
19. Ofori E, DeKosky ST, Febo M, et al. Free-water imaging of the hippocampus is a sensitive marker of Alzheimer's disease. *Neuroimage Clin* 2019;24:101985.
20. Hoy AR, Ly M, Carlsson CM, et al. Microstructural white matter alterations in preclinical Alzheimer's disease detected using free water elimination diffusion tensor imaging. *PLoS One* 2017;12(3):e0173982.
21. Montal V, Vilaplana E, Alcolea D, et al. Cortical microstructural changes along the Alzheimer's disease continuum. *Alzheimers Dement* 2018;14:340-351.
22. Ofori E, Pasternak O, Planetta P, et al. Longitudinal changes in free-water within the substantia nigra of Parkinson's disease. *Brain* 2015;138:2322-2331.
23. Pasternak O, Kubicki M, Shenton ME. In vivo imaging of neuroinflammation in schizophrenia. *Schizophr Res* 2016;173:200-212.
24. Sone D, Shigemoto Y, Ogawa M, et al. Association between neurite metrics and tau/inflammatory pathology in Alzheimer's disease. *Alzheimers Dement* 2020;12(1):e12125.
25. Hoy AR, Koay CG, Kecskemeti SR, et al. Optimization of a free water elimination two-compartmental model for diffusion tensor imaging. *NeuroImage* 2014;103:323-333.
26. Henriques RN, Rokem A, Garyfallidis E, St-Jean S, et al. Optimization of a free water elimination two-compartment model for diffusion tensor imaging. *ReScience* 2017;3:2.
27. Veraart J, Fieremans E, Novikov DS Diffusion MRI noise mapping using random matrix theory. *Magn Reson Med*. 2016;76(5):1582-1593.
28. Ashburner J. A fast diffeomorphic image registration algorithm. *Neuroimage* 2007;38:95-113.
29. Gonzalez-Escamilla G, Lange C, Teipel S, et al. PETPVE12: an SPM toolbox for partial volume effects correction in brain PET – Application to amyloid imaging with AV45-PET. *Neuroimage* 2017;147:669-677.
30. Matsuda H, Yamao T. Software development for quantitative analysis of brain amyloid PET. *Brain Behavior* 2022:E2499.
31. Amadoru S, Doré V, McLean CA, et al. Comparison of amyloid PET measured in Centiloid units with neuropathological findings in Alzheimer's disease. *Alzheimers Res Ther* 2020;12:22.
32. Mathotaarachchi S, Wang S, Shin M, et al. VoxelStats: a MATLAB package for multi-modal voxel-wise brain image analysis. *Front Neuroinform* 2016;10:20.
33. Xia M, Wang J, He Y. BrainNet Viewer: a network visualization tool for human brain connectomics. *PLoS One* 2013;8:e68910.
34. Shigemoto Y, Sone D, Imabayashi E, et al. Dissociation of tau deposits and brain atrophy in early Alzheimer's disease: a combined positron emission tomography/magnetic resonance imaging study. *Front Aging Neurosci* 2018;10:223.
35. Ittner A, Ittner LM. Dendritic tau in Alzheimer's disease. *Neuron* 2018;99:13-27.
36. Ossenkoppele R, Schonhaut DR, Schöll M, et al. Tau PET patterns mirror clinical and neuroanatomical variability in Alzheimer's disease. *Brain* 2016;139:1551-1567.

37. Harada R, Okamura N, Furumoto S, et al. Correlations of 18F-THK5351 PET with postmortem burden of tau and astrogliosis in Alzheimer disease. *J Nucl Med* 2018;59:671-674.
38. Ji F, Pasternak O, Ng KK, et al. White matter microstructural abnormalities and default network degeneration are associated with early memory deficit in Alzheimer's disease continuum. *Sci Rep* 2019;9:4749.
39. Ji F, Pasternak O, Liu S, et al. Distinct white matter microstructural abnormalities and extracellular water increases relate to cognitive impairment in Alzheimer's disease with and without cerebrovascular disease. *Alzheimers Res Ther* 2017;9:63.
40. Bergamino M, Walsh RR, Stokes AM. Free-water diffusion tensor imaging improves the accuracy and sensitivity of white matter analysis in Alzheimer's disease. *Sci Rep* 2021;11:1-12.
41. Hulette CM, Welsh-Bohmer KA, Murray MG, et al. Neuropathological and neuropsychological changes in "normal" aging: evidence for preclinical Alzheimer disease in cognitively normal individuals. *J Neuropathol Exp Neurol* 1998;57:1168-74.
42. van der Kall LM, Truong T, Burnham SC, et al. Association of β-amyloid level, clinical progression, and longitudinal cognitive change in normal older individuals. *Neurology* 2021;96:e662-670.
43. Arriagada PV, Marzloff K, Hyman BT. Neurofibrillary tangles but not senile plaques parallel duration and severity of Alzheimer's disease. *Neurology* 1992;42:631-639.
44. Wischik CM, Harrington CR, Storey JM. Tau-aggregation inhibitor therapy for Alzheimer's disease. *Biochem Pharmacol* 2014;88:529-539.
45. Giannakopoulos P, Herrmann FR, Bussiere T, et al. Tangle and neuron numbers, but not amyloid load, predict cognitive status in Alzheimer' s disease. *Neurology* 2003;60:1495-1500.
46. Weston PS, Simpson IJ, Ryan NS, et al. Diffusion imaging changes in grey matter in Alzheimer's disease: a potential marker of early neurodegeneration. *Alzheimers Res Ther* 2015;7:47.
47. Chao LL, DeCarli C, Kriger S, et al. Associations between white matter hyperintensities and β amyloid on integrity of projection, association, and limbic fiber tracts measured with diffusion tensor MRI. *PLoS One.* 2013;8(6):e65175.
48. Racine AM, Adluru N, Alexander AL, et al. Associations between white matter microstructure and amyloid burden in preclinical Alzheimer's disease: a multimodal imaging investigation. *NeuroImage Clin* 2014;4:604-614.
49. Dong JW, Jelescu IO, Ades-Aron B, et al. Diffusion MRI biomarkers of white matter microstructure vary nonmonotonically with increasing cerebral amyloid deposition. *Neurobiol Aging* 2020;89:118-128.
50. Lee P, Kim HR, Jeong Y Detection of gray matter microstructural changes in Alzheimer's disease continuum using fiber orientation. *BMC Neurol* 2020;20:1-10.
51. Braak H, Alafuzoff I, Arzberger T, et al. Staging of Alzheimer disease-associated neurofibrillary pathology using paraffin sections and immunocytochemistry. *Acta Neuropathol* 2006;112:389-404.
52. Andica C, Kamagata K, Hatano T, et al. Free-water imaging in white and gray matter in Parkinson's disease. *Cells.* 2019;8(8):839.
53. Metzler-Baddeley C, O'Sullivan MJ, Bells S, et al. How and how not to correct for CSF-contamination in diffusion MRI. *Neuroimage* 2012;59:1394-1403.
54. Pasternak O, Westin CF, Bouix S, et al. Excessive extracellular volume reveals a neurodegenerative pattern in schizophrenia onset. *J Neurosci* 2012;32:17365-17372.
55. Heneka MT, Carson, EIK, et al. Neuroinflammation in Alzheimer's disease. *Lancet Neurol* 2015;14:388-405.
56. Harada R, Okamura N, Furumoto S, et al. 18F-THK5351: a novel PET radiotracer for imaging neurofibrillary pathology in Alzheimer's disease. *J Nucl Med* 2016;57:208-214.
57. Bergmann Ø, Henriques R, Westin CF, et al. Fast and accurate initialization of the free-water imaging model parameters from multi-shell diffusion MRI. *NMR Biomed* 2020;33:e4219.
58. Ball G, Srinivasan L, Aljabar P, et al. Development of cortical microstructure in the preterm human brain. *Proc Natl Acad Sci U S A.* 2013;110(23):9541-6.
59. Hoy AR, Ly M, Carlsson CM, et al. Microstructural white matter alterations in preclinical Alzheimer's disease detected using free water elimination diffusion tensor imaging. *PLoS One.* 2017;12(3):e0173982.

SUPPORTING INFORMATION

Additional supporting information can be found online in the Supporting Information section at the end of this article.

How to cite this article: Nakaya M, Sato N, Matsuda H, et al. Free water derived by multi-shell diffusion MRI reflects tau/neuroinflammatory pathology in Alzheimer's disease. *Alzheimer's Dement.* 2022;8:e12356.
https://doi.org/10.1002/trc2.12356